Research Square

Preprints are preliminary reports that have not undergone peer review.
They should not be considered conclusive, used to inform clinical practice,
or referenced by the media as validated information.

Biology-Informed Titer Estimation from CHO Cell Morphology

Yiming Yang
Jiangnan University
Xiaoping Jiang
Jiangnan University
Hailin Yang
bioprocessor@126.com
Jiangnan University
Qiong Wang
Wuxi People's Hospital
Shidong Shi
Innovent Biologics (Suzhou) Co., Ltd

Research Article

Keywords: CHO cells, cell morphology, image analysis, titer estimation, apparent specific productivity

Posted Date: November 16th, 2026

DOI: https://doi.org/10.21203/rs.3.rs-11595077/v1

License: This work is licensed under a Creative Commons Attribution 4.0 International License.
Read Full License

Additional Declarations: No competing interests reported.

Biology-Informed Titer Estimation from CHO Cell Morphology

Yiming Yang[a], Xiaoping Jiang[b]

[a] *School of Biotechnology, Jiangnan University, Wuxi, 214122, China*

[b] *School of Biotechnology, Jiangnan University, Wuxi, 214122, China*

**Corresponding author: bioprocessor@126.com (Hailin Yang, Tel: +86-180-6151-9905), Address: Jiangnan University, Wuxi, China, 214122*

wangqiong_john@163.com (Qiong Wang), Address: Wuxi People's Hospital, Wuxi, China, 214043

shidong.shi@innoventbio.com (Shidong Shi), Address: Innovent Biologics (Suzhou) Co., Ltd., Suzhou, China, 215123

Abstract

Offline product titer measurements provide intermittent snapshots of product accumulation in Chinese hamster ovary (CHO) cell cultures. We extracted geometric and population heterogeneity features from phase-contrast microscopy images of CHO cultures producing the same antibody product. We examined morphological dynamics and their batch-level associations with production performance. Eight training batches supported association analysis and model development. Model performance was assessed by leave-one-batch-out cross-validation (LOBO) and evaluation on a held-out batch (T1). Changes in cell circularity and aspect ratio were significantly correlated with Day 12 (D12) titer, with Spearman correlation coefficients of 0.881 and −0.905, respectively. A composite morphology score was used to estimate apparent specific productivity. Measured titer was used to derive training $q_{P,\mathrm{app}}$ targets, not as a prediction input. Day-specific biology-informed structured models combined these estimates with measured integrated viable cell density (IVCD) to estimate contemporaneous titer on Day 10 (D10) and D12. The D10 and D12 structured models achieved coefficients of determination (R^2) of 0.866 and 0.904, respectively, in LOBO cross-validation. The corresponding relative titer errors in T1 were 1.21% and 1.00%. Together, these findings indicate that combining morphological analysis with integrated viable cell density provides a biologically interpretable approach to late-culture titer estimation and shows potential for bioprocess monitoring and production performance assessment.

Keywords: CHO cells; cell morphology; image analysis; titer estimation; apparent specific productivity

1. Introduction

Chinese hamster ovary (CHO) cells are widely used mammalian host cells for recombinant therapeutic protein production, and fed-batch culture is an important approach for achieving high cell densities and high levels of protein expression [1-4]. However, CHO cell culture is jointly influenced by medium composition, feeding strategy, cellular metabolic state, and other factors, which may lead to differences in cell growth and final production performance across culture batches [5-11]. Cell density, viability, glucose, and lactate remain important indicators for assessing culture status. With advances in process analytical technology, online sensors, spectroscopic analysis, and data-driven models have increasingly been applied to cell culture monitoring [12-17]. Although these technologies provide multiple routes for real-time assessment of culture status, further use of cell morphology to support the characterization of culture status and production performance remains of research interest.

Microscopy image analysis provides a new source of information for quantitatively characterizing cell state. Cell segmentation and image feature extraction yield measurements of cell area, size, contour shape, and optical texture, allowing morphological changes in cell populations during culture to be described [18]. Previous studies have linked CHO cell size changes to culture stage, cell cycle, and recombinant protein production capacity; changes in the culture environment may also affect cell volume and population morphology [19-22]. In addition, microscopy-based morphological analysis has been used to assess antibody production performance in CHO cells and to identify morphological differences between clones with different production phenotypes [23-26]. These studies indicate that morphological features can reflect the structural characteristics of cell populations and may provide information on cellular states related to production capacity. However, relationships between single-cell morphology and production performance depend on culture conditions, feature definitions, analytical scale, and other factors. Morphological differences at the cell level cannot be directly equated with differences in production performance at the batch level.

Jiang et al. used cell geometric and optical texture features to develop non-invasive random forest soft-sensor models that estimated culture-state indicators, including viable cell density (VCD), glucose, and lactate [27]. Other studies have used morphological features to assess antibody production capacity in CHO cells and explored the prediction of production performance during culture using machine learning and multivariate analysis [23, 28, 29]. However, existing studies differ in their emphasis on estimating culture-state indicators and predicting cellular production performance. The relationship between morphological dynamics and batch production capacity, and the use of biologically meaningful production-capacity indicators to support late-culture titer estimation, warrant further investigation. From a fermentation biology perspective, product accumulation depends on cell number and its changes during culture and is also closely related to specific cellular productivity. Combining morphological information with apparent specific productivity and integrated viable cell density may therefore provide a biologically interpretable modeling approach for late-culture titer estimation.

This study characterized the relationship between CHO cell morphological dynamics and batch production performance and developed late-culture titer estimation models. First, we quantified cell geometry and population heterogeneity across batches and evaluated associations between core morphological metrics and titer. Second, we estimated apparent specific productivity from morphological features to link cellular phenotypes with batch-level production performance. Third, we combined these estimates with integrated viable cell density (IVCD) in separate biology-informed structured models for Day 10 (D10) and Day 12 (D12). Each model used morphological information available on or before its target day and IVCD over the corresponding period. We evaluated performance using leave-one-batch-out cross-validation (LOBO) and holdout-batch evaluation, with the process-variable baseline and direct morphological regression models as comparators.

2. Materials and methods

2.1. Cell culture and offline measurements

This study included data from nine independent CHO cell culture batches obtained using an industrial cell line supplied by Innovent Biologics (Suzhou) Co., Ltd., all grown in fed-batch culture in 2 L benchtop bioreactors. Eight batches formed the main-analysis set (S1–S8), and one formed the holdout-analysis set (T1). All nine batches were used to produce the same antibody product. Multiple anonymized process strategies were used across the batches; batch information and titer measurements are presented in Table 1. To ensure consistent interbatch comparisons, measured D12 titer was used as the common endpoint for the primary association analysis. The last available titer measurement was collected on D12 or D13, depending on the batch, and is reported as final titer. Morphological observations were available through D13 for all nine batches.

Table 1 CHO cell culture batch information and titer measurements

Batch ID	Process strategy	Day 12 titer (mg/L)	Final titer (mg/L)
S1	A	2729	2629
S2	B	9638	9868
S3	C	10488	10488
S4	D	10972	10972
S5	E	10429	10429
S6	F	8887	9099
S7	G	10053	10053
S8	A	2671	2591
T1	H	11741	11741

Note: Final titer denotes the last available titer measurement, obtained on D12 or D13 depending on the batch.

Culture samples were collected aseptically every 24 h for immediate offline physiological and biochemical measurements under the established measurement protocol and for phase-contrast microscopy. Offline measurements characterized cell growth and biochemical status during culture, whereas microscopy images were used for cell segmentation and morphological feature extraction. To simulate sparse late-culture titer measurements in industrial production, titer was measured primarily during late culture.

The principal instruments used for offline measurement of CHO cell physiological indicators, biochemical parameters, and product titer are listed in Table 2.

Table 2 Instruments and corresponding parameters for offline measurements in CHO cell culture

Parameter	Instrument	Manufacturer (country)
Viable cell density (VCD)	Automated cell counter	Beckman Coulter (USA)
Cell viability	Automated cell counter	Beckman Coulter (USA)
Glucose concentration	Automated biochemical analyzer	Roche (Switzerland)
Lactate concentration	Automated biochemical analyzer	Roche (Switzerland)
Ammonium concentration	Automated biochemical analyzer	Roche (Switzerland)
Osmolality	Blood gas analyzer	Medica (USA)
Product titer	HPLC system	Agilent (USA)

2.2. Morphological feature analysis

2.2.1. Microscopy image acquisition and cell segmentation

Culture samples were collected at the scheduled time points for phase-contrast imaging of CHO cells using a NEXCOPE NE900 upright phase-contrast microscope (Novel Optics, China) equipped with a 10× eyepiece and a 40× phase-contrast objective. The pixel resolution under these conditions was 0.05 μm/pixel. All images were saved in a high-resolution lossless format and organized by batch and sampling time.

An in-house-trained deep learning semantic segmentation network (HRNet) processed the original phase-contrast images to generate binary cell masks and identify cell contours. Segmentation results were linked to the original images, culture batches, and culture days for subsequent morphological feature extraction. The image-processing workflow was developed with reference to previous CHO cell morphology studies [27, 30].

2.2.2. Single-cell morphological feature extraction

Single-cell contours were extracted from segmentation masks to calculate geometric features, including cell area, perimeter, equivalent diameter, circularity, and aspect ratio. The analysis focused on morphological metrics describing contour regularity, elongation, and population size dispersion.

For cell i, let A_i and P_i denote its contour area and perimeter, respectively, and let $L_{\mathrm{major},i}$ and $L_{\mathrm{minor},i}$ denote the major and minor axis lengths obtained by ellipse fitting. Circularity and aspect ratio were defined as follows:

$$\mathrm{Circ}_i = \frac{4\pi A_i}{P_i^2}$$

$$\mathrm{AR}_i = \frac{L_{\mathrm{major},i}}{L_{\mathrm{minor},i}}$$

Equivalent diameter was calculated from the cell contour area:

$$d_i = 2\sqrt{\frac{A_i}{\pi}}$$

Circularity describes how closely a two-dimensional cell contour approximates an ideal circle; aspect ratio describes contour elongation; and equivalent diameter expresses the size corresponding to the projected cell area.

2.2.3. Morphological quality control and construction of batch-level features

To improve the consistency of cell morphological measurements, segmentation results were filtered according to the established quality-control (QC) procedure. Because abnormally small objects may include cell debris and segmentation artifacts, objects with areas < 50 μm² were excluded, and only objects with areas ≥ 50 μm² were retained for subsequent morphological statistics. The same filtering criterion was applied to all culture batches to reduce the influence of abnormal segmentation objects on cell geometric and population heterogeneity metrics.

Single-cell morphological features were summarized by culture batch and day to construct daily morphological metrics. Circularity was represented by the median to reduce the influence of morphologically abnormal objects, and aspect ratio by the arithmetic mean to characterize overall contour elongation in the cell population. The diameter coefficient of variation (CV), calculated as the sample standard deviation of equivalent diameter divided by its mean, described relative size heterogeneity in the cell population. These metrics were calculated as follows:

$$\mathrm{Circ}_{b,d} = \mathrm{median}_{i \in \mathcal{I}_{b,d}}(\mathrm{Circ}_i)$$

Here, $\mathcal{I}_{b,d}$ denotes the set of cell objects included in the statistics for batch b on culture day d.

The daily mean aspect ratio was calculated as follows:

$$\overline{\mathrm{AR}}_{b,d} = \frac{1}{n_{b,d}} \sum_{i=1}^{n_{b,d}} \mathrm{AR}_i$$

Here, $n_{b,d}$ is the number of cell objects included for the corresponding batch and culture day.

For batch b on culture day d, let $\bar{d}_{b,d}$ and $\mathrm{SD}_{b,d}$ denote the mean and standard deviation of equivalent diameter, respectively. The diameter coefficient of variation was defined as follows:

$$CV_{b,d} = \frac{\mathrm{SD}_{b,d}}{\bar{d}_{b,d}}$$

The D6–D10 interval was selected to capture morphological remodeling during mid-to-late culture. The D8–D13 window was used to describe later changes in population size heterogeneity [25, 29, 31-33]. The robust median was used for circularity because its distribution was skewed. Three core batch-level morphological metrics were constructed. Metrics A and B were the D10−D6 changes in median circularity and mean aspect ratio, respectively. Metric C was the mean daily diameter CV from D8 through the specified day, using valid observation days. C10 and C12 were used for D10 and D12 estimation, respectively; C12 also supported D12 association analysis. C13 was used only for descriptive analysis. These metrics characterize

changes in contour regularity, elongation, and population size dispersion during culture, respectively. Metrics A, B, and C were calculated as follows:

$$A_b = \mathrm{Circ}_{b,10} - \mathrm{Circ}_{b,6}$$

$$B_b = \overline{\mathrm{AR}}_{b,10} - \overline{\mathrm{AR}}_{b,6}$$

$$C_{b,t} = \frac{1}{|D_{b,t}|} \sum_{d \in D_{b,t}} CV_{b,d}$$

Here, $D_{b,t}$ denotes the set of culture days with valid morphological observations for batch b from D8 to the target culture day t.

2.3. Data analysis and titer estimation

2.3.1. Data organization

All data were organized by culture batch and day, and single-cell morphological features passing quality control were summarized into daily and batch-level metrics. Independent culture batches were the basic statistical units. Multiple cell objects within a batch were not treated as independent biological replicates, avoiding inflation of statistical evidence through pseudoreplication.

2.3.2. Associations between batch-level morphological metrics and production performance

To investigate the relationship between CHO cell morphological dynamics and batch production performance, eight independent culture batches were used as the analytical units to evaluate associations of the three core morphological metrics with measured Day-12 (D12) titer and apparent specific productivity separately. Apparent specific productivity ($q_{\mathrm{P,app}}$) was calculated from product titer and integrated viable cell density to characterize apparent product formation per unit of cumulative viable cell density.

Spearman rank correlation quantified the direction and strength of monotonic associations between each morphological metric and production performance. Statistical significance was assessed using two-sided exact permutation tests and Holm correction for multiple testing [34]. The correlation coefficient was calculated as follows:

$$\rho_s = \mathrm{corr}(\mathrm{rank}(X_b), \mathrm{rank}(Y_b))$$

Here, X_b denotes a core morphological metric for batch b, Y_b is the corresponding measured D12 titer or apparent specific productivity, $rank(\cdot)$ denotes rank transformation, and $corr(\cdot)$ is the Pearson correlation coefficient between the two ranked variables.

Because the study included only eight independent training batches, two-sided P values for the correlation tests were calculated using exact permutation tests. Production-performance values were exhaustively permuted across the corresponding batches while the observed morphological metrics were held fixed to construct the null distribution of correlation coefficients and assess the statistical significance of the observed correlation.

Holm correction was applied separately to the three associations with D12 titer and the three associations with apparent specific productivity (m = 3 per family). Adjusted P values < 0.05 were considered statistically significant. Spearman correlation coefficients, raw P values, and Holm-adjusted P values were reported. The correction was calculated as follows:

$$p_{(i)}^{\mathrm{Holm}} = \min\left\{1,\ \max_{1\le j\le i}\left[(m-j+1)p_{(j)}\right]\right\}$$

Here, $p_{(j)}$ denotes the raw P values sorted in ascending order, and m is the number of tests in the same family.

2.3.3. Calculation and morphology-based estimation of apparent specific productivity

To establish a quantitative link between cell morphological features and product formation capacity during culture, apparent specific productivity ($q_{\mathrm{P,app}}$) was introduced as an intermediate descriptor. Apparent specific productivity at the target culture day was calculated for each batch from the relationship between product titer and integrated viable cell density (IVCD) [35, 36].

First, integrated viable cell density up to the target culture day was calculated by trapezoidal integration of the measured viable cell density (VCD) of each culture batch:

$$IVCD_{b,t} = \sum_{k=1}^{n_{b,t}-1} \frac{VCD_{b,k} + VCD_{b,k+1}}{2}(d_{k+1} - d_k)$$

Here, $IVCD_{b,t}$ denotes integrated viable cell density for batch b through culture day t; ($VCD_{b,k}$) is the viable cell density at the kth actual observation time point; d_k is the corresponding culture time; and $n_{b,t}$ is the number of valid observation points included in the integration.

Batch-level apparent specific productivity was calculated from the measured titer at the target culture day and the corresponding IVCD:

$$q_{P,\mathrm{app},b,t} = \frac{T_{b,t}}{IVCD_{b,t}}$$

Here, $T_{b,t}$ is the measured titer of batch b on culture day t. When titer is expressed in mg/L, VCD in 10^6 cells/mL, and time in days, apparent specific productivity is expressed in pg/(cell·day). This metric describes the apparent level of product accumulation per unit of cumulative viable cell density; it is not an independently measured instantaneous single-cell specific productivity.

To further explore the quantitative relationship between cell morphological features and apparent specific productivity, three core morphological metrics, circularity change, aspect ratio change, and diameter coefficient of variation, were selected to construct a composite morphology score. Metrics A and B characterize dynamic changes in contour regularity and elongation, respectively, whereas metric C describes population size heterogeneity. Because the three morphological metrics differ in scale and distribution, each was first standardized using its mean and sample standard deviation in the model training batches:

$$Z_{j,b} = \frac{X_{j,b} - \mu_{j,\mathrm{train}}}{s_{j,\mathrm{train}}}$$

Here, $X_{j,b}$ denotes the morphological metric for batch b indexed by j; $\mu_{j,\text{train}}$ and $s_{j,\text{train}}$ are the mean and sample standard deviation of that metric in the corresponding training batches, respectively.

An equally weighted composite morphology score was constructed using fixed directional weights for the three core metrics:

$$S_{b,t} = \frac{Z_{A,b} - Z_{B,b} - Z_{C,b,t}}{3}$$

Ordinary least squares (OLS) regression with an intercept was then used to establish a linear relationship between the composite morphology score and apparent specific productivity:

$$\hat{q}_{P,\text{app},b,t} = \beta_{0,t} + \beta_{1,t} S_{b,t}$$

Here, $\hat{q}_{P,\text{app},b,t}$ is the apparent specific productivity estimated from morphological information, and $\beta_{0,t}$ and $\beta_{1,t}$ are the intercept and regression coefficient of the model for the target culture day, respectively. The model used the three fixed core morphological metrics and directional weights, without additional feature selection or hyperparameter optimization.

During model training, the regression target was the apparent specific productivity calculated from measured titer and integrated viable cell density in the training batches. During model application, apparent specific productivity was estimated using only the morphological features of the batch being evaluated, without using its measured titer as a model input. In each LOBO round, standardization parameters and regression coefficients were fitted using seven training batches and applied to the remaining batch. For T1 evaluation, the model was fitted using all eight training batches.

2.3.4. Morphology-based titer estimation and model comparison

D10 and D12 were selected as estimation time points because measured titer, morphology, and viable cell density were available during mid-to-late culture. D10 represented an intermediate late-culture time point, whereas D12 provided a common later endpoint. Each model used only information available on or before its target day.

Based on the relationship between product accumulation and integrated viable cell density, the biology-informed structured model combined morphology-estimated apparent specific productivity with the integrated viable cell density corresponding to the target culture day to estimate titer quantitatively. The model was expressed as follows:

$$\hat{T}_{b,t} = \hat{q}_{P,\text{app},b,t} \times IVCD_{b,t}$$

Here, $\hat{T}_{b,t}$ denotes the estimated titer of batch b on culture day t; $\hat{q}_{P,\text{app},b,t}$ is the apparent specific productivity estimated from morphological features; $IVCD_{b,t}$ is integrated viable cell density through the target culture day; and t takes values of 10 and 12.

To account for information availability at different culture time points, the D10 and D12 models used the same modeling framework, but separate apparent specific productivity estimation models were constructed for each target day. Circularity change and aspect ratio change were both based on morphological information

from D6–D10, whereas diameter CV was summarized over D8–D10 and D8–D12 for the D10 and D12 models, respectively.

Two types of direct regression model were included as comparators to evaluate the performance of different modeling strategies. The process-variable baseline model directly estimated titer at the target culture day using predefined process-related features, providing a performance reference based on conventional process information. The input features and fixed configurations of the comparison models are provided in Supplementary Fig. S1. The direct morphological regression model used ridge regression with a fixed configuration to map morphological features directly to titer [37]. In contrast to these direct regression approaches, the biology-informed structured model used apparent specific productivity as an intermediate variable, combining cell morphological information with integrated viable cell density to characterize product formation per unit of cumulative viable cell density.

2.4. Software statement

The segmentation algorithms, morphological data acquisition and processing, quality control, statistical analysis, and regression modeling used in this study were implemented in Python 3.13.14. All programs were run on a 64-bit Windows 11 operating system.

3. Results and discussion

3.1. Image segmentation and morphological data quality control

To obtain cell contour information for morphological analysis, an HRNet-based image segmentation method was used to process phase-contrast images of CHO cells, and the area distributions of segmented objects and differences among batches were evaluated. As shown in Fig. 1a, segmentation identified the main cell contours in microscopic fields with different cell densities and displayed the spatial distribution of individual objects through segmentation masks, providing a basis for subsequent extraction of single-cell morphological features.

Object areas were analyzed in eight training batches and one holdout batch, yielding a total of 26,233 segmented objects. The object area distribution was heterogeneous (Fig. 1b). After excluding segmented objects with areas below 50 μm², 16,670 objects remained, accounting for approximately 63.5% of all objects. The proportion meeting this area threshold ranged from 53.6% to 69.4% among batches (Fig. 1c), indicating differences in the size composition of segmented objects across batches. Such differences may reflect both actual cellular morphology and image segmentation performance.

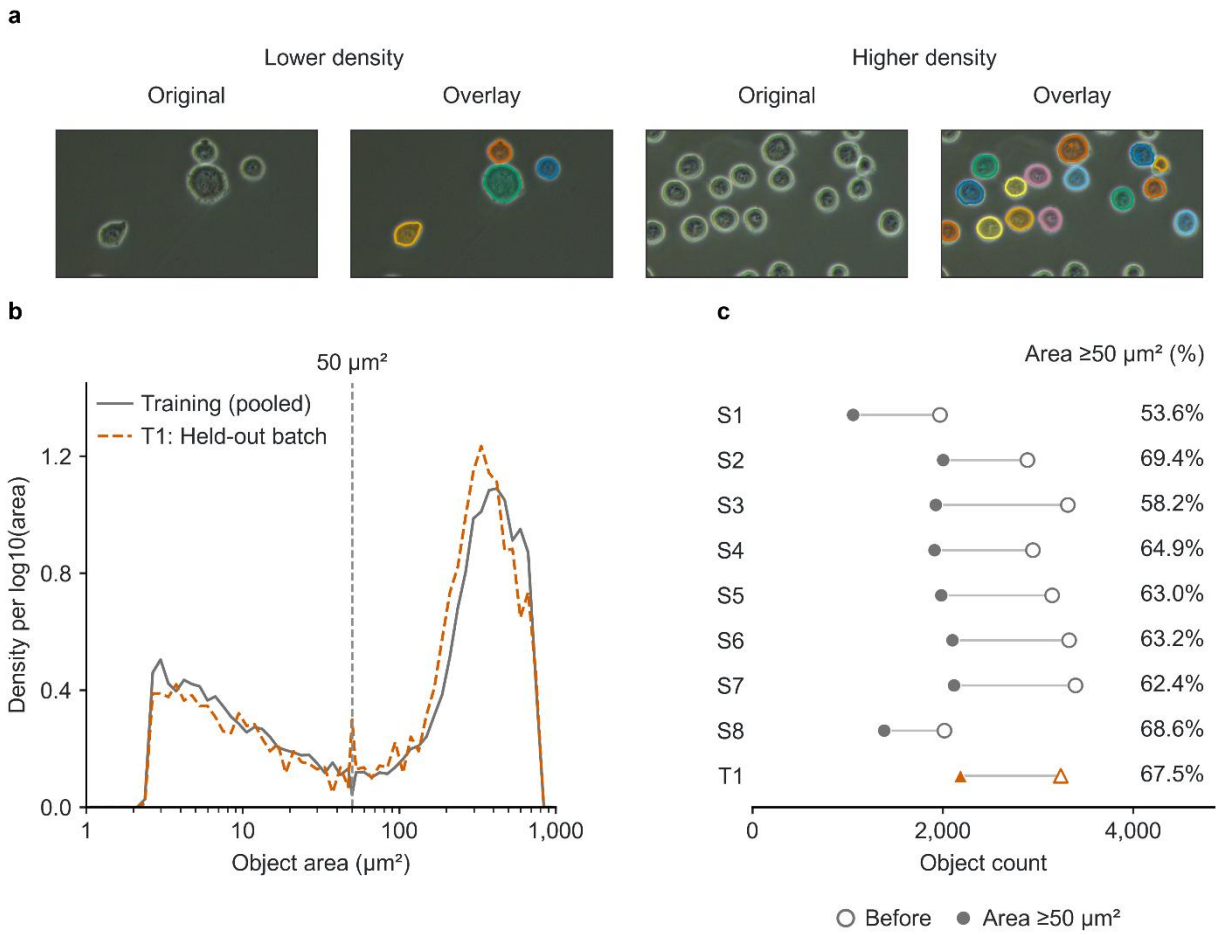


Fig. 1 Examples of CHO cell microscopy image segmentation and object area distributions. a, Representative phase-contrast images at different cell densities with colored segmentation overlays identifying cell contours. b, Area distributions of segmented objects from the eight training batches and holdout batch T1. The dashed line marks the 50 µm² threshold. c, Object counts and area characteristics by batch. Open and filled symbols denote all recorded objects and those with areas ≥ 50 µm², respectively; percentages on the right indicate the proportions meeting this criterion. Circles denote training batches and triangles denote T1. Across nine batches, 26,233 segmented objects were recorded, of which 16,670 had areas ≥ 50 µm²

3.2. Morphological dynamics during CHO cell culture and their biological significance

To examine morphological changes during CHO cell culture, morphological data collected over D1–D13 from eight training batches and one holdout batch were analyzed, comprising 117 batch-day morphological observations (Fig. 2).

Cell circularity changed dynamically with culture time across batches (Fig. 2a). Circularity decreased during mid-culture in some batches and then gradually recovered, although the magnitude and timing of these changes differed among batches. Aspect ratio also fluctuated with time: some batches showed higher aspect ratios during mid-culture, followed by gradual decreases during subsequent culture (Fig. 2b).

In addition to changes in cell contours, the size distribution within cell populations showed marked dynamics. As shown in Fig. 2c, the diameter coefficient of variation (CV) followed different trajectories among batches, with substantial fluctuations during mid-to-late culture in some batches. These findings suggest that population size heterogeneity may change during culture and that mean cell size alone does not fully describe morphological differences within the population [38].

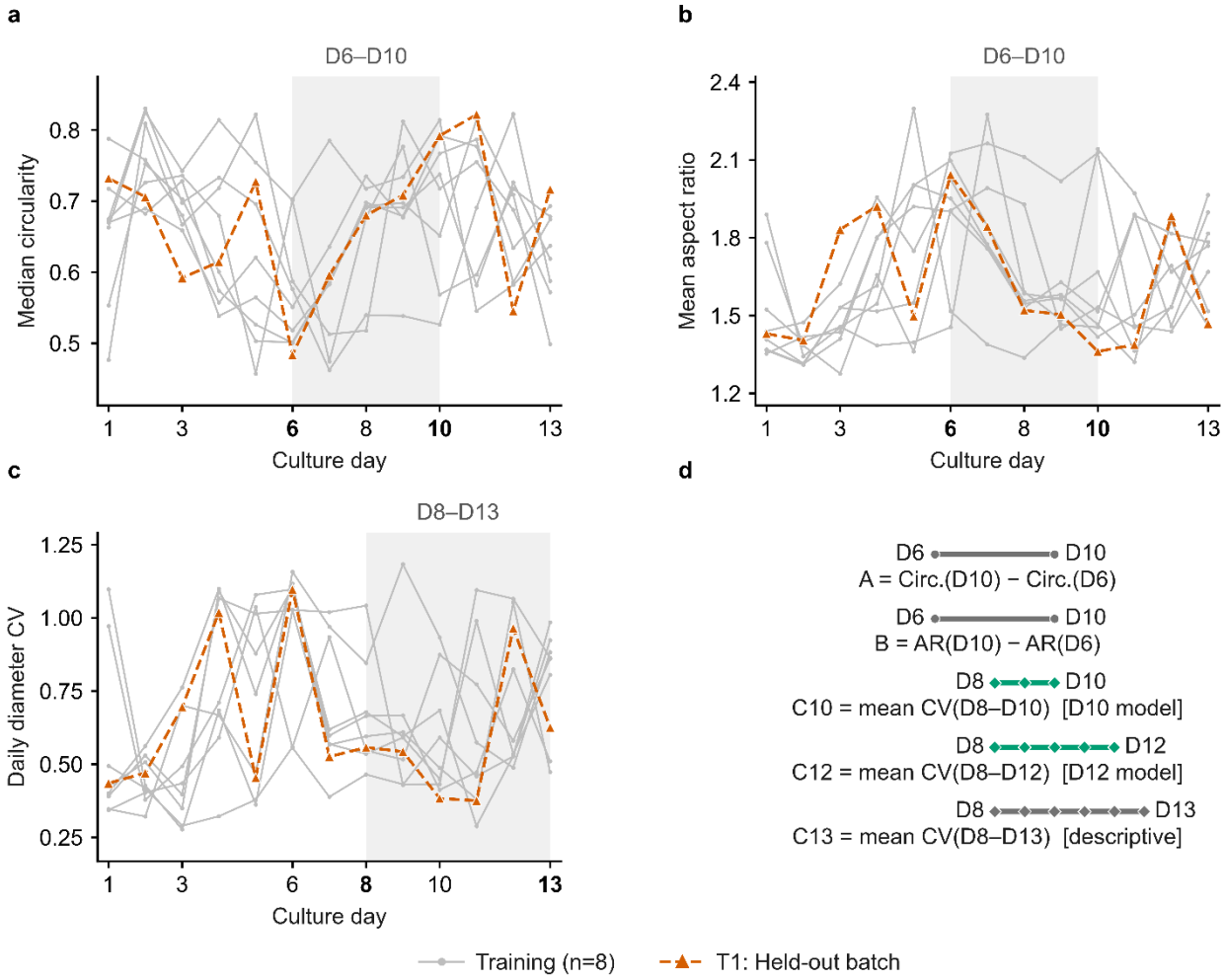


Fig. 2 Morphological dynamics and feature construction during CHO cell culture. a–c, Daily median circularity, mean aspect ratio, and diameter coefficient of variation (CV), respectively, over D1–D13 in eight training batches (S1–S8) and holdout batch T1. Each trajectory represents an independent culture batch. Gray solid lines with circles denote training batches; the orange dashed line with triangles denotes T1. Light-gray shading marks D6–D10 in a and b and D8–D13 in c. d, Core metric definitions and time windows. A and B are D10−D6 changes in median circularity and mean aspect ratio, respectively. C_{10} and C_{12} are arithmetic means of daily diameter CV over D8–D10 and D8–D12, respectively, used for titer estimation on the corresponding target days. C_{12} also supports D12 production-performance association analysis. C_{13} averages daily diameter CV over D8–D13 for descriptive analysis only. CV summaries use days with valid morphological observations within each window. Diameter CV was calculated from cell equivalent diameter. Circ., circularity; AR, aspect ratio

These changes have a physiological context. In a study of CHO fed-batch culture, Pan et al. [21] observed that a marked phase of cell size increase could still occur after proliferation slowed, accompanied by an increase in specific antibody productivity. Lloyd et al. [32] also reported a relationship between cell size and specific recombinant protein productivity, suggesting that cell growth and product formation capacity may not be fully synchronized. In addition, Alhuthali et al. [31] found that changes in culture osmolality could affect CHO cell volume, growth, and antibody production performance, while differences in cell-cycle state might also contribute to cell size regulation. These studies suggest that the morphological dynamics observed here may reflect the combined effects of cellular growth state and the culture environment.

Based on these observations, circularity change metric A and aspect ratio change metric B over D6–D10, together with mean diameter CV metric C over a defined culture window, were selected to describe contour

regularity, elongation, and population size heterogeneity, respectively (Fig. 2d). The CV summary over D8–D13 was used to describe morphological changes over a longer culture window, whereas the D12 model used CV information available through D12 to align morphological characterization with the titer estimation time point.

3.3. Associations between core morphological metrics and batch production performance

After characterizing CHO cell morphological dynamics, we further evaluated the relationships between the core morphological metrics and batch production performance. Using eight independent training batches as the statistical units, we analyzed the associations of circularity change (metric A), aspect ratio change (metric B), and diameter CV over D8–D12 (metric C_{12}) with measured D12 titer. Statistical evaluation used Spearman rank correlation, two-sided exact permutation tests, and Holm correction for multiple testing (Fig. 3).

Circularity change (metric A) was significantly positively correlated with measured D12 titer, with a Spearman correlation coefficient ρ of 0.881 and a Holm-adjusted P value of 0.0145 (Fig. 3a). Aspect ratio change (metric B) was significantly negatively correlated with D12 titer, with $\rho = -0.905$ and an adjusted P value of 0.0137 (Fig. 3b). These results indicate that, among the training batches in this study, batches with greater increases in circularity and greater decreases in aspect ratio over D6–D10 generally had higher D12 titers.

Geometrically, increased circularity and decreased aspect ratio may both reflect a shift toward relatively regular, less elongated cell contours. Both associations with titer were consistent with this geometric interpretation. Using morphological profiling of CHO cells, Hisada et al. [33] found that morphological information could characterize and predict changes in antibody production performance. By combining transcriptomics with Cell Painting analysis, Nelson et al. [25] further identified associated molecular and morphological features in CHO cells with different production capacities. These studies provide support for evaluating production performance using cellular morphological phenotypes.

Compared with the two shape-change metrics, diameter CV (metric C_{12}) was negatively correlated with D12 titer ($\rho = -0.714$), but its Holm-adjusted P value of 0.0576 did not meet the predefined criterion for statistical significance (Fig. 3c). Diameter CV reflects relative size dispersion within the cell population, and its changes may be associated with cell growth state, cell-cycle composition, and differences in the culture environment. Previous studies have reported relationships among cell size, the cell cycle, and CHO cell productivity [21, 22]. Size heterogeneity may therefore contain some production-related information, although the specific cellular physiological processes involved could not be determined in this study.

We further analyzed the relationships between the three core metrics and apparent specific productivity (Fig. 3d). Circularity change (metric A) was positively correlated with apparent specific productivity ($\rho = 0.810$), whereas aspect ratio change (metric B) and diameter CV (metric C_{12}) were negatively correlated ($\rho = -0.786$ and -0.810, respectively). The association directions for all three metrics were consistent with

those in the D12 titer analysis, but all corresponding Holm-adjusted P values were 0.0653 and did not reach statistical significance.

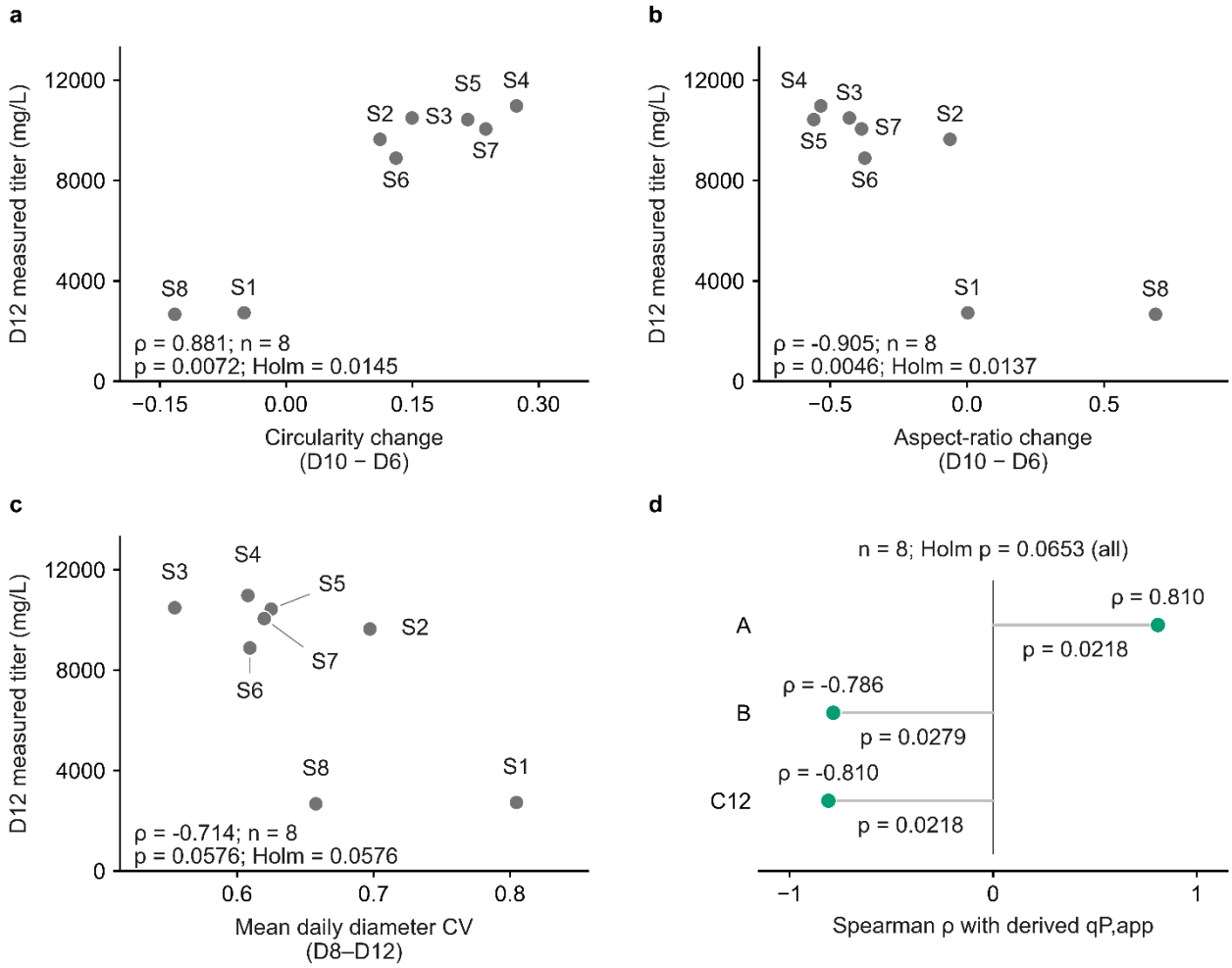


Fig. 3 Associations between core morphological metrics and CHO cell production performance. a–c, Associations of measured D12 titer with circularity change A, aspect ratio change B, and mean daily diameter coefficient of variation (CV) over D8–D12 (C_{12}), respectively. Each point represents an independent training batch (S1–S8, $n = 8$). Spearman rank correlation (ρ) quantifies association direction and strength; P values were obtained by two-sided exact permutation tests. Holm correction was applied separately to the three titer tests and the three apparent specific productivity tests. d, Correlations of A, B, and C_{12} with apparent specific productivity ($q_{P,app}$). Points show ρ, and horizontal segments connect each coefficient to zero rather than indicating uncertainty. Panel d labels report ρ and unadjusted P values. Reference $q_{P,app}$ was calculated as measured D12 titer divided by integrated viable cell density (IVCD) over D1–D12; it is a derived indicator, not a directly measured instantaneous single-cell production rate

Overall, circularity change was positively associated with D12 titer, whereas aspect ratio change was negatively associated. Diameter CV showed a negative association that did not reach significance after Holm correction. Together, these findings identify contour dynamics as informative batch-level phenotypes associated with production performance.

3.4. Estimation of apparent specific productivity from morphological information

To further evaluate the value of morphological information for quantitatively characterizing production-related capacity in CHO cells, we combined the three core morphological metrics into a composite

morphology score and estimated apparent specific productivity using ordinary least squares (OLS) regression. Apparent specific productivity calculated from measured D12 titer and the corresponding integrated viable cell density (IVCD) was used as the reference. Model performance was evaluated by LOBO in the eight training batches (Fig. 4).

Reference apparent specific productivity ranged from approximately 18.7 to 43.9 pg/(cell·day) across the training batches, indicating differences in product accumulation per unit of cumulative viable cell density. The model based on the composite morphology score captured the main trend in reference apparent specific productivity, with a LOBO mean absolute error (MAE) of 2.98 pg/(cell·day) and a root mean square error (RMSE) of 4.14 pg/(cell·day) (Fig. 4a). Additional evaluation of the D12 model in a single holdout batch yielded an absolute apparent specific productivity estimation error of 0.48 pg/(cell·day), corresponding to a relative titer error of 1.00%.

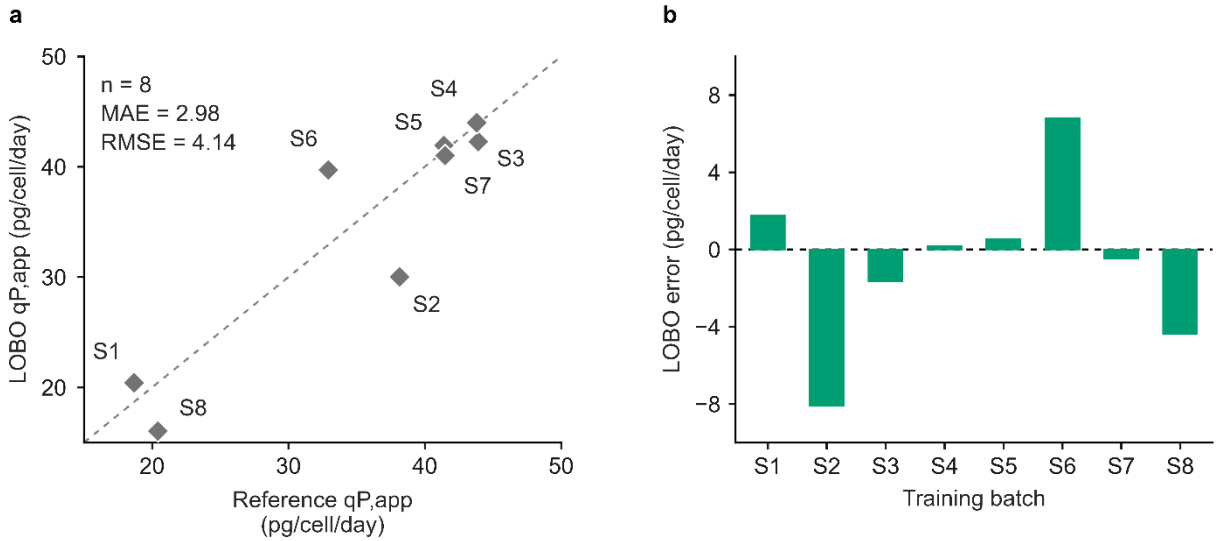


Fig. 4 Estimation of apparent specific productivity from cell morphological features. a, Reference apparent specific productivity versus estimates from the composite morphology score. Reference values were calculated as measured D12 titer divided by integrated viable cell density (IVCD) over D1–D12. Estimates were obtained by leave-one-batch-out cross-validation (LOBO) across eight independent training batches (S1–S8); holdout batch T1 was excluded. Each diamond represents a batch, the dashed line indicates equality, and mean absolute error (MAE) and root mean square error (RMSE) are reported. b, Signed out-of-fold errors (estimate minus reference) for S1–S8; the horizontal dashed line marks zero. The model relates the fixed-direction composite morphology score based on A, B, and C_{12} to apparent specific productivity using ordinary least squares regression. Standardization parameters and regression coefficients were determined within each training fold. Apparent specific productivity and errors are expressed in pg/(cell·day)

Out-of-fold errors varied among batches, with relatively large deviations in S2 and S6 (Fig. 4b). To interpret these estimates biologically, we considered evidence that specific productivity is not determined solely by cell proliferation [39]. Through studies of cell-cycle regulation, Bi et al. [40] found that cell volume and some components associated with protein synthesis could still increase when cell proliferation was inhibited, accompanied by increased antibody productivity per cell. Together with previous studies of cell size and productivity [19, 21], these findings suggest that morphological states observed during culture may partly reflect cellular physiological changes associated with product formation.

Compared with previous studies that used microscopy-derived morphological features to estimate culture-state variables such as viable cell density, glucose, and lactate [27], this study further used morphological information to characterize apparent specific productivity associated with product formation, extending morphological analysis from culture-state description to quantitative estimation of production-related capacity [36].

3.5. Titer estimation on culture Day 10 and comparison of modeling strategies

We next extended the morphology-based productivity framework to contemporaneous titer estimation on culture Day 10 (D10). Three modeling strategies were compared: a process-variable baseline model, a direct morphological regression model, and a biology-informed structured model (Fig. 5). The structured model estimated apparent specific productivity from the composite morphology score and then calculated titer using IVCD up to the target day. The input features and fixed configurations of each model are provided in Supplementary Fig. S1.

In LOBO cross-validation of the eight training batches, the process-variable baseline model performed best, with a coefficient of determination (R^2) of 0.9944 and an MAE of 212.9 mg/L. The direct morphological regression model had an R^2 of 0.4395 and an MAE of 1856.7 mg/L, indicating relatively large out-of-fold estimation errors when titer was fitted directly from morphological features. By comparison, the structured model achieved an R^2 of 0.8658 and reduced MAE to 1038.7 mg/L (Fig. 5a; Supplementary Fig. S2). The structured model captured the main differences in titer levels among training batches, although estimation deviations remained in some batches (Fig. 5b).

In the single holdout batch T1, measured D10 titer was 11,017 mg/L. The process-variable baseline and direct morphological regression models yielded estimates of 9442.70 and 10,641.50 mg/L, with relative errors of 14.29% and 3.41%, respectively. The structured model estimated a titer of 11,150.54 mg/L, differing from the measured titer by 133.54 mg/L, with a relative error of 1.21% (Fig. 5c, d). Complete evaluation results for all models are provided in Supplementary Fig. S2.

The process-variable baseline achieved high accuracy in cross-validation of the training batches, indicating that conventional culture-process data effectively characterized interbatch differences related to titer. By comparison, direct regression of titer using morphological features alone may not fully describe the combined effects of cell state and viable cell abundance during product accumulation.

From a bioprocess perspective, product titer depends on production capacity per cell and the cumulative viable cell density during culture. Previous studies have reported relationships among CHO cell growth, cell size changes, and productivity per cell, but cell proliferation and product formation are not always synchronized [19, 21, 31]. By estimating apparent specific productivity from morphology and using measured IVCD, the structured model represents production-related state and cumulative cell abundance separately. This gives the titer estimate a clear biological interpretation.

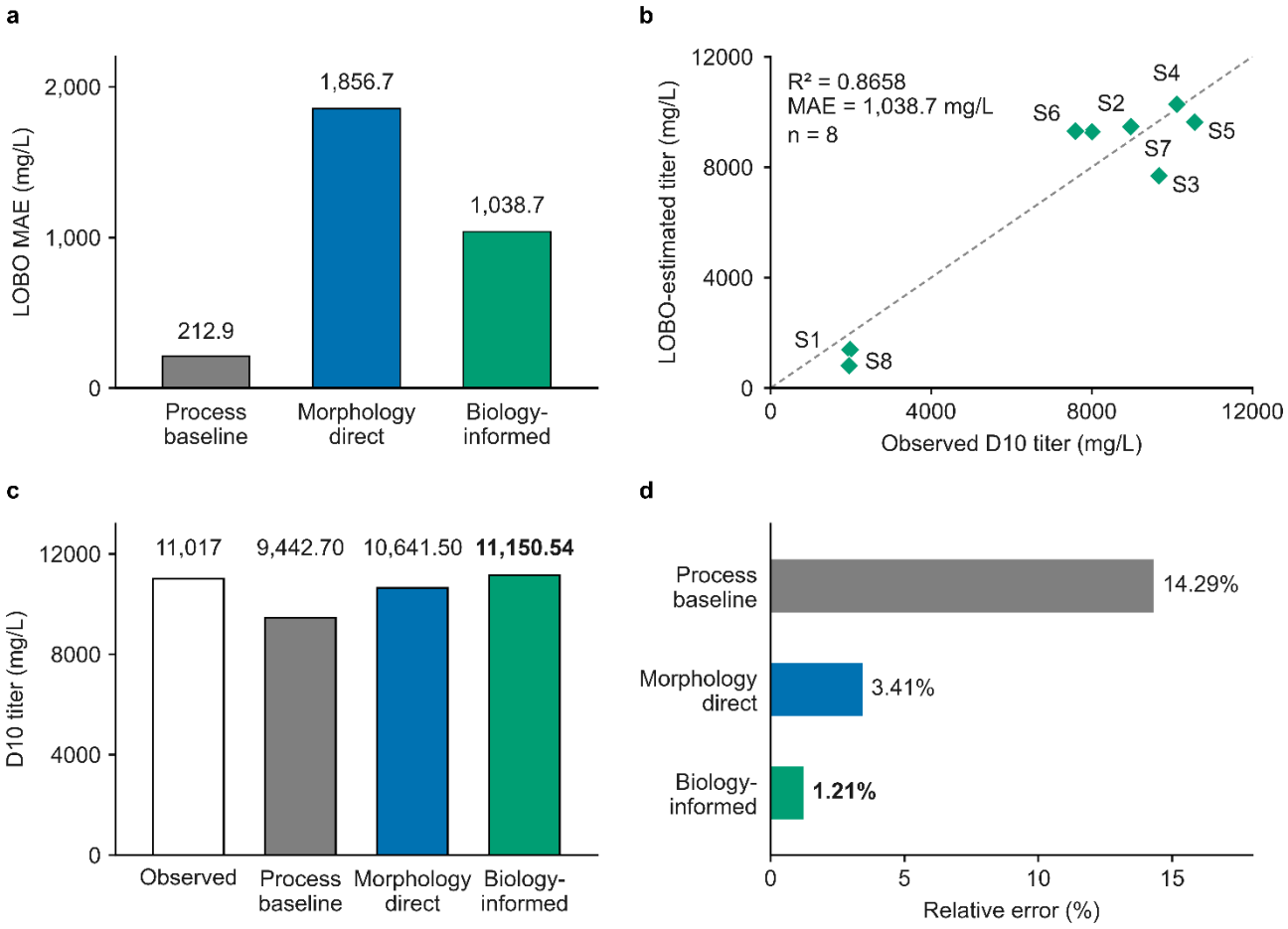


Fig. 5 Model comparison and validation for contemporaneous D10 titer estimation. a, Leave-one-batch-out cross-validation (LOBO) mean absolute error (MAE) for the process-variable baseline model, direct morphological regression model, and biology-informed structured model in eight independent training batches (S1–S8). Model-wise LOBO R^2 values are provided in Supplementary Fig. S2. b, Measured D10 titers and out-of-fold estimates from the structured model; diamonds denote batches, and the dashed line indicates equality. R^2 and MAE are reported. c, Measured D10 titer and estimates from all three models for the single holdout batch T1. d, Absolute relative errors for T1, defined as the absolute estimate–measurement difference divided by measured titer and expressed as percentages. The structured model combines apparent specific productivity estimated from circularity and aspect ratio changes over D6–D10 and mean daily diameter coefficient of variation over D8–D10 (C_{10}) with measured integrated viable cell density (IVCD) through D10. Titer and MAE are expressed in mg/L

Combining morphology with measured IVCD reduced D10 estimation error relative to direct morphological regression and yielded a low error in T1. These results support contemporaneous D10 titer estimation using the structured framework and provide a basis for morphology-assisted production monitoring.

3.6. Titer estimation on culture Day 12 and applicability at different culture time points

Following D10 titer estimation, we applied the same structured modeling framework to culture Day 12 (D12) to evaluate its applicability at a later culture stage (Fig. 6). The D12 model retained circularity change and aspect ratio change and used mean diameter CV over D8–D12 to characterize population size heterogeneity during late culture. The composite score formulation and validation principles remained the same, but regression parameters were fitted separately to the D12 data.

In LOBO cross-validation of the eight training batches, the D12 structured model achieved an R^2 of 0.904 and an MAE of 674.6 mg/L, outperforming the direct morphological regression model ($R^2 = 0.473$, MAE = 1628.8 mg/L) and approaching the performance of the process-variable baseline model ($R^2 = 0.942$, MAE = 588.2 mg/L) (Fig. 6a; Supplementary Fig. S2). Out-of-fold estimates from the structured model generally reflected titer differences among the training batches, with an RMSE of approximately 1008 mg/L (Fig. 6b).

In holdout batch T1, measured D12 titer was 11,741 mg/L. The process-variable baseline and direct morphological regression models yielded estimates of 10,140.80 and 11,152.19 mg/L, with relative errors of 13.63% and 5.02%, respectively. The structured model estimated a titer of 11,858.42 mg/L, with an absolute error of 117.42 mg/L and a relative error of approximately 1.00% (Fig. 6c). The low error in T1 further supports late-culture titer estimation using the biology-informed structured framework.

Together, the D10 and D12 results show that the structured framework captured batch-level titer differences and achieved low errors in holdout batch T1. Separate regression parameters were fitted at each target day within the same framework.

Biologically, CHO cells may undergo changes in proliferation, size, and production-related states during culture, and increases in cell abundance and product formation capacity may not be synchronized across physiological states [19, 21]. Changes in the culture environment may also affect cell volume, growth, and antibody production performance [22]. These physiological considerations provide a context for evaluating the framework separately at each culture time point.

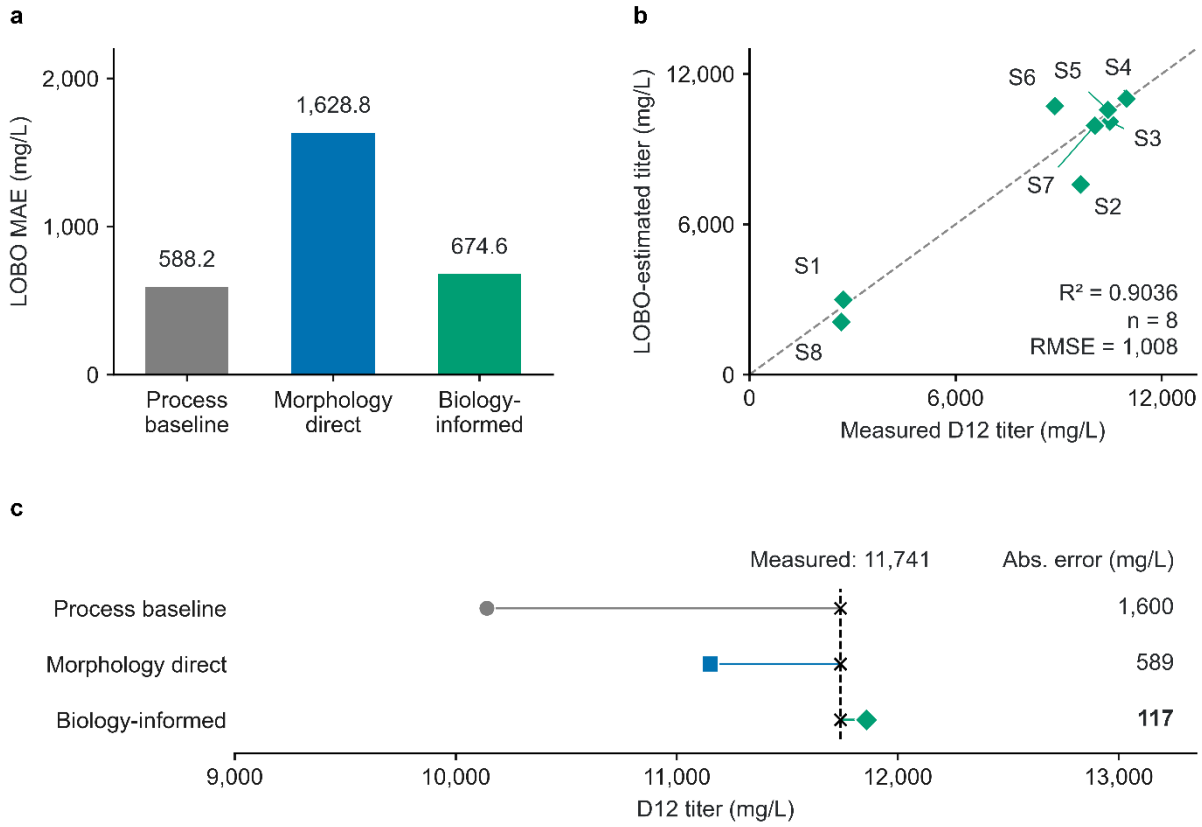


Fig. 6 Model comparison and applicability assessment for contemporaneous D12 titer estimation. a, Leave-one-batch-out cross-validation (LOBO) mean absolute error (MAE) for the process-variable baseline model, direct morphological regression model, and biology-informed structured model in eight independent training batches (S1–S8). Model-wise LOBO R^2 and relative errors for holdout batch T1 are provided in Supplementary Fig. S2. b, Measured D12 titers and out-of-fold estimates from the structured model; diamonds denote batches, and the dashed line indicates equality. Root mean square error (RMSE) is reported. c, Measured titer and model estimates for the single holdout batch T1. Crosses and the vertical dashed line mark the measured value; colored markers denote estimates, and values on the right give absolute errors. The structured model uses circularity change A, aspect ratio change B (both D10−D6), and C_{12} (mean daily diameter coefficient of variation over D8–D12) with measured integrated viable cell density (IVCD) over D1–D12. Titer and errors are expressed in mg/L

4. Conclusions

Using data from nine independent CHO cell culture batches, this study established an analytical framework encompassing characterization of cell morphological dynamics, associations with batch production performance, estimation of apparent specific productivity, and titer estimation. Circularity, aspect ratio, and population size heterogeneity changed dynamically during culture, with distinct morphological trajectories among batches. Batch-level association analysis showed that circularity change was significantly positively correlated with measured D12 titer, whereas aspect ratio change was significantly negatively correlated, suggesting that cell contour dynamics may contain biological information related to production performance. We then combined the three core morphological metrics into a composite morphology score to quantitatively estimate apparent specific productivity and developed a biology-informed structured model by

incorporating integrated viable cell density (IVCD). The separately fitted D10 and D12 structured models achieved LOBO R^2 values of 0.866 and 0.904, respectively. Their relative errors in holdout batch T1 were 1.21% and 1.00%, respectively. The structured model outperformed direct morphological regression at both evaluation time points but did not exceed the process-variable baseline in cross-validation of the training batches. These findings show that cell morphological information provides quantitative support for characterizing production-related states in CHO cells and, when combined with cumulative viable cell density, supports titer estimation at different evaluation time points during mid-to-late culture.

This study is limited by the small number of independent culture batches and the incomplete coverage of production-related physiological indicators. Future work could include additional independent culture batches and integrate indicators of the cell cycle, metabolic state, and protein synthesis to further clarify the biological relationships between morphological changes and production capacity and evaluate the applicability of the structured model across cell lines and culture conditions. Integration of morphological information with process parameters could also be explored to provide more reliable technical support for monitoring production state and estimating titer in CHO cell culture.

Highlights

- A morphology-informed approach is developed for CHO cell titer estimation.
- Morphological dynamics reveal batch-level associations with product titer.
- Composite morphology scores estimate apparent specific productivity.
- Biology-informed modeling integrates morphology with viable cell accumulation.
- Structured modeling outperforms direct morphological regression.

Statements and Declarations

Data confidentiality and anonymization

Due to confidentiality agreements, actual batch identifiers and process parameters are not disclosed in this study. Relevant data were normalized, and the same data-desensitization procedures were consistently applied to all figures and tables.

Ethics approval and consent to participate

Not applicable.

Consent for publication

Not applicable.

Data availability

The datasets generated and analyzed during the current study are not publicly available due to confidentiality agreements regarding the company's proprietary industrial process parameters, but are available from the corresponding author on reasonable request.

Competing interests

The authors declare that they have no financial or non-financial interests that are directly or indirectly related to the work submitted for publication.

Funding

This work was supported by the National Key Research and Development Program of China (2022YFC3401304); the National Natural Science Foundation of China (32471540, 32371540, 21878128, and 31701582).

Authors' contributions

Y.Y. designed and conducted the experiments, developed the algorithms and models, performed the formal data analysis, and was responsible for writing, reviewing, and editing the manuscript. X.J. assisted with data collection and curation. H.Y. and Q.W. contributed to conceptualization, funding acquisition, and project supervision. S.S. was responsible for data review and provided the experimental conditions for this study. All authors read and approved the final manuscript.

Acknowledgements

The authors would like to thank Innovent Biologics (Suzhou) Co., Ltd. for generously providing the proprietary CHO-K1 cell line and sharing the experimental conditions used in this study.

References

[1] Harrington C, et al. Production of butyrate and branched-chain amino acid catabolic byproducts by CHO cells in fed-batch culture enhances their specific productivity. Biotechnol Bioeng. 2021;118(12):4786–4799. https://doi.org/10.1002/bit.27942

[2] Handlogten MW, et al. Intracellular response to process optimization and impact on productivity and product aggregates for a high-titer CHO cell process. Biotechnol Bioeng. 2018;115(1):126–138. https://doi.org/10.1002/bit.26460

[3] Ha TK, et al. Factors affecting the quality of therapeutic proteins in recombinant Chinese hamster ovary cell culture. Biotechnology Advances. 2022;54:107831. https://doi.org/10.1016/j.biotechadv.2021.107831

[4] Xu W-J, et al. Progress in fed-batch culture for recombinant protein production in CHO cells. Applied Microbiology and Biotechnology. 2023;107(4):1063–1075. https://doi.org/10.1007/s00253-022-12342-x

[5] Liang G, et al. Soft-sensor model development for CHO growth/production, intracellular metabolite, and glycan predictions. Front Mol Biosci. 2024;11:1441885. https://doi.org/10.3389/fmolb.2024.1441885

[6] Jarusintanakorn S, et al. Determination of Chinese hamster ovary (CHO) cell densities and antibody titers from small volumes of cell culture supernatants using multivariate analysis and partial least squares regression of UV-Vis spectra. Anal Bioanal Chem. 2021;413(23):5743–5753. https://doi.org/10.1007/s00216-021-03549-4

[7] Li B, et al. Performance monitoring of a mammalian cell based bioprocess using Raman spectroscopy. Anal Chim Acta. 2013;796:84–91. https://doi.org/10.1016/j.aca.2013.07.058

[8] Yan X, et al. Development of an in-line Raman analytical method for commercial-scale CHO cell culture process monitoring: influence of measurement channels and batch number on model performance. Biotechnology Journal. 2024;19(1):2300395. https://doi.org/10.1002/biot.202300395

[9] Zhu Z, et al. Understanding the effect of temperature downshift on CHO cell growth, antibody titer and product quality by intracellular metabolite profiling and in vivo monitoring of redox state. Biotechnol Prog. 2023;39(4):e3352. https://doi.org/10.1002/btpr.3352

[10] Rish AJ, Drennen JK, Anderson CA. Metabolic trends of Chinese hamster ovary cells in biopharmaceutical production under batch and fed-batch conditions. Biotechnol Prog. 2022;38(1):e3220. https://doi.org/10.1002/btpr.3220

[11] Tung M, et al. High intracellular seed train BiP levels correlate with poor production culture performance in CHO cells. Biotechnology Journal. 2018;13(10):1700746. https://doi.org/10.1002/biot.201700746

[12] Ji X, et al. Characterization of cell cycle and apoptosis in Chinese hamster ovary cell culture using flow cytometry for bioprocess monitoring. Biotechnol Prog. 2022;38(1):e3211. https://doi.org/10.1002/btpr.3211

[13] Toussaint C, Henry O, Durocher Y. Metabolic engineering of CHO cells to alter lactate metabolism during fed-batch cultures. J Biotechnol. 2016;217:122–131. https://doi.org/10.1016/j.jbiotec.2015.11.010

[14] Mulukutla BC, et al. Metabolic engineering of Chinese hamster ovary cells towards reduced biosynthesis and accumulation of novel growth inhibitors in fed-batch cultures. Metabolic Engineering. 2019;54:54–68. https://doi.org/10.1016/j.ymben.2019.03.001

[15] Qin J, et al. The effect of hyperosmolality application time on production, quality, and biopotency of monoclonal antibodies produced in CHO cell fed-batch and perfusion cultures. Applied Microbiology and Biotechnology. 2019;103(3):1217–1229. https://doi.org/10.1007/s00253-018-9555-7

[16] Fung Shek C, Betenbaugh M. Taking the pulse of bioprocesses: at-line and in-line monitoring of mammalian cell cultures. Current Opinion in Biotechnology. 2021;71:191–197. https://doi.org/10.1016/j.copbio.2021.08.007

[17] Metze S, et al. Monitoring online biomass with a capacitance sensor during scale-up of industrially relevant CHO cell culture fed-batch processes in single-use bioreactors. Bioprocess and Biosystems Engineering. 2020;43(2):193–205. https://doi.org/10.1007/s00449-019-02216-4

[18] Romanova N, et al. Hyperosmolality in CHO culture: Effects on cellular behavior and morphology. Biotechnol Bioeng. 2021;118(6):2348–2359. https://doi.org/10.1002/bit.27747

[19] Helfer A, et al. Tuning metabolic efficiency for increased product yield in high titer fed-batch Chinese hamster ovary cell culture. Biotechnol Prog. 2023;39(3):e3327. https://doi.org/10.1002/btpr.3327

[20] Ritacco FV, Wu Y, Khetan A. Cell culture media for recombinant protein expression in Chinese hamster ovary (CHO) cells: history, key components, and optimization strategies. Biotechnol Prog. 2018;34(6):1407–1426. https://doi.org/10.1002/btpr.2706

[21] Pan X, et al. Metabolic characterization of a CHO cell size increase phase in fed-batch cultures. Applied Microbiology and Biotechnology. 2017;101(22):8101–8113. https://doi.org/10.1007/s00253-017-8531-y

[22] Seewöster T, Lehmann J. Cell size distribution as a parameter for the predetermination of exponential growth during repeated batch cultivation of CHO cells. Biotechnol Bioeng. 1997;55(5):793–797. https://doi.org/10.1002/(SICI)1097-0290(19970905)55:5%3C793::AID-BIT9%3E3.0.CO;2-6

[23] Gyorgypal A, et al. Evaluating the impact of media and feed combinations on CHO cell culture performance and monoclonal antibody (trastuzumab) production. Cytotechnology. 2025;77(1):40. https://doi.org/10.1007/s10616-024-00690-7

[24] Huang YM, et al. Maximizing productivity of CHO cell-based fed-batch culture using chemically defined media conditions and typical manufacturing equipment. Biotechnol Prog. 2010;26(5):1400–1410. https://doi.org/10.1002/btpr.436

[25] Nelson L, et al. Transcriptomics and cell painting analysis reveals molecular and morphological features associated with fed-batch production performance in CHO recombinant clones. Biotechnol Bioeng. 2023;120(11):3177–3190. https://doi.org/10.1002/bit.28518

[26] Shi J, et al. Accelerating biopharmaceutical cell line selection with label-free multimodal nonlinear optical microscopy and machine learning. Commun Biol. 2025;8(1):157. https://doi.org/10.1038/s42003-025-07596-w

[27] Jiang X, et al. Morphology-driven non-invasive soft sensors for Chinese hamster ovary cell cultivation. Systems Microbiology and Biomanufacturing. 2026;6(3):95. https://doi.org/10.1007/s43393-026-00493-1

[28] Tao W, et al. Selection of high-producing clones by a relative titer predictive model using image analysis. Ann Transl Med. 2021;9(14):1144. https://doi.org/10.21037/atm-21-2822
[29] Pan X, et al. Transcriptome analysis of CHO cell size increase during a fed-batch process. Biotechnology Journal. 2019;14(3):1800156. https://doi.org/10.1002/biot.201800156
[30] Wang J, et al. Deep High-Resolution Representation Learning for Visual Recognition. IEEE Trans Pattern Anal Mach Intell. 2021;43(10):3349–3364. https://doi.org/10.1109/TPAMI.2020.2983686
[31] Alhuthali S, Kotidis P, Kontoravdi C. Osmolality effects on CHO cell growth, cell volume, antibody productivity and glycosylation. International Journal of Molecular Sciences. 2021;22(7):3290. https://doi.org/10.3390/ijms22073290
[32] Lloyd DR, et al. Relationship between cell size, cell cycle and specific recombinant protein productivity. Cytotechnology. 2000;34(1–2):59–70. https://doi.org/10.1023/A:1008103730027
[33] Hisada T, et al. Prediction of antibody production performance change in Chinese hamster ovary cells using morphological profiling. Journal of Bioscience and Bioengineering. 2024;137(6):453–462. https://doi.org/10.1016/j.jbiosc.2024.01.011
[34] Aickin M, Gensler H. Adjusting for multiple testing when reporting research results: the Bonferroni vs Holm methods. Am J Public Health. 1996;86(5):726–728. https://doi.org/10.2105/AJPH.86.5.726
[35] Pan X, et al. Selection of chemically defined media for CHO cell fed-batch culture processes. Cytotechnology. 2017;69(1):39–56. https://doi.org/10.1007/s10616-016-0036-5
[36] Mahé A, et al. Exploring the limits of conventional small-scale CHO fed-batch for accelerated on demand monoclonal antibody production. Bioprocess and Biosystems Engineering. 2022;45(2):297–307. https://doi.org/10.1007/s00449-021-02657-w
[37] Hoerl AE, Kennard RW. Ridge regression: Biased estimation for nonorthogonal problems. Technometrics. 1970;12(1):55–67. https://doi.org/10.1080/00401706.1970.10488634
[38] Romanova N, et al. Single-cell analysis of CHO cells reveals clonal heterogeneity in hyperosmolality-induced stress response. Cells. 2022;11(11):1763. https://doi.org/10.3390/cells11111763
[39] Du Z, et al. Use of a small molecule cell cycle inhibitor to control cell growth and improve specific productivity and product quality of recombinant proteins in CHO cell cultures. Biotechnol Bioeng. 2015;112(1):141–155. https://doi.org/10.1002/bit.25332
[40] Bi JX, Shuttleworth J, Al-Rubeai M. Uncoupling of cell growth and proliferation results in enhancement of productivity in p21CIP1-arrested CHO cells. Biotechnol Bioeng. 2004;85(7):741–749. https://doi.org/10.1002/bit.20025